

Learning Bloch Simulations for MR Fingerprinting by Invertible Neural Networks

Fabian Balsiger^{1,2*}[0000-0001-7577-9870], Alain Jungo^{1,2*}[0000-0001-8327-4653],
Olivier Scheidegger³, Benjamin Marty^{4,5}, and Mauricio Reyes^{1,2}

- ¹ ARTORG Center for Biomedical Research, University of Bern, Bern, Switzerland
[fabian.balsiger|alain.jungo]@artorg.unibe.ch
- ² Insel Data Science Center, Inselspital, Bern University Hospital, Bern, Switzerland
- ³ Support Center for Advanced Neuroimaging (SCAN), Institute for Diagnostic and Interventional Neuroradiology, Inselspital, Bern University Hospital, Bern, Switzerland
- ⁴ NMR Laboratory, Institute of Myology, Neuromuscular Investigation Center, Paris, France
- ⁵ NMR Laboratory, CEA, DRF, IBFJ, MIRCen, Paris, France

Abstract. Magnetic resonance fingerprinting (MRF) enables fast and multiparametric MR imaging. Despite fast acquisition, the state-of-the-art reconstruction of MRF based on dictionary matching is slow and lacks scalability. To overcome these limitations, neural network (NN) approaches estimating MR parameters from fingerprints have been proposed recently. Here, we revisit NN-based MRF reconstruction to jointly learn the forward process from MR parameters to fingerprints and the backward process from fingerprints to MR parameters by leveraging invertible neural networks (INNs). As a proof-of-concept, we perform various experiments showing the benefit of learning the forward process, i.e., the Bloch simulations, for improved MR parameter estimation. The benefit especially accentuates when MR parameter estimation is difficult due to MR physical restrictions. Therefore, INNs might be a feasible alternative to the current solely backward-based NNs for MRF reconstruction.

Keywords: Reconstruction · Magnetic resonance fingerprinting · Invertible neural network.

1 Introduction

Magnetic resonance fingerprinting (MRF) [16] is a relatively new but increasingly used [20] concept for fast and multiparametric quantitative MR imaging. Acquisitions of MRF produce unique magnetization evolutions per voxel, called fingerprints, due to temporal varying MR sequence schedules. From these fingerprints, MR parameters (e.g., relaxation times) are then reconstructed using a dictionary matching, comparing each fingerprint to a dictionary of simulated fingerprints with known MR parameters. Although the MRF acquisition itself

* These authors contributed equally and are listed by flipping a coin.

is fast thanks to high undersampling, the dictionary matching is slow, discrete and cannot interpolate, and lacks scalability with increasing number of MR parameters.

With the advent of deep learning, neural networks (NNs) have been explored to overcome the limitations of the dictionary matching. The dictionary matching can be formulated as a regression problem from the fingerprints to the MR parameters. Several methods have been applied to MRF with impressive results both in terms of reconstruction accuracy and speed [8,13,10,19,4,12,21,14,11,3]. Among these, spatially regularizing methods trained on *in vivo* MRF acquisitions showed superiority over methods performing fingerprint-wise regression [5,10,4,3,11,14]. However, spatial methods might require a considerable amount of training data to achieve reasonable robustness for highly heterogeneous diseases [3]. Therefore, robust fingerprint-wise methods, leveraging the dictionaries for training, are required to alleviate the need of *in vivo* MRF acquisitions.

We revisit NN-based MRF reconstruction by formulating it as an inverse problem where we jointly learn the forward process from MR parameters to fingerprints and the backward process from fingerprints to MR parameters. In doing so, the available information of the forward process is leveraged, which might help disentangling MR physical processes and consequently improve the MR parameter estimation of the backward process. To this end, we leverage invertible neural networks (INNs) [9]. As proof-of-concept, we perform various experiments showing the benefit of learning the forward process, i.e., the Bloch simulations, for improved NN-based MRF reconstruction.

2 Methodology

2.1 MR Fingerprinting using Invertible Neural Networks

Inverse problems are characterized by having some observations \mathbf{y} , from which we want to obtain the underlying parameters \mathbf{x} . The forward process $\mathbf{y} = f(\mathbf{x})$ is usually well defined and computable. However, the backward process $\mathbf{x} = f^{-1}(\mathbf{y})$ is not trivial to compute. MRF can be formulated as an inverse problem [7]. The forward process f is described by the Bloch equations [6]. Meaning, from some MR parameters $\mathbf{x} \in \mathbb{R}^M$, one can simulate a corresponding fingerprint $\mathbf{y} \in \mathbb{C}^T$ for a given MRF sequence. The backward process f^{-1} in MRF is typically solved by dictionary matching, or recently via regression by NNs. However, in doing so, the knowledge of the well-defined forward process is completely omitted in the backward process. We hypothesize that by leveraging the knowledge of the forward process, NN-based MRF reconstruction can be improved. Therefore, we aim at jointly learning the forward and the backward process by using INNs. Once learned, the trained INN can be used to estimate MR parameters \mathbf{x} from a fingerprint \mathbf{y} , as done in literature.

Fig. 1 depicts INNs in the context of MRF. Given training pairs (\mathbf{x}, \mathbf{y}) from a dictionary, the MR parameters \mathbf{x} are fed into the INN, which predicts the fingerprint $\hat{\mathbf{y}}$. Optimizing a mean squared error (MSE) loss between \mathbf{y} and $\hat{\mathbf{y}}$ results in learning the forward process. Feeding the fingerprint \mathbf{y} from the opposite

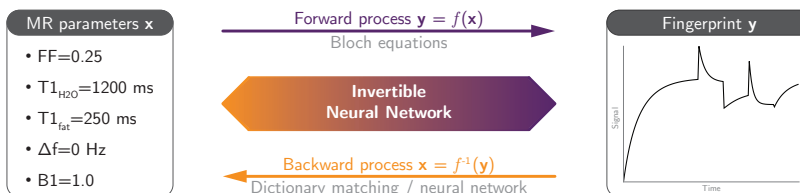


Fig. 1. Overview of the INN in the context of MRF. The forward process simulates fingerprints \mathbf{y} from MR parameters \mathbf{x} , usually by Bloch simulations. The backward process estimates MR parameters \mathbf{x} of a fingerprint \mathbf{y} , usually by dictionary matching or recently NNs. The INN is capable of doing both the forward and backward process.

direction into the INN predicts the MR parameters $\hat{\mathbf{x}}$. Here, we also optimize a MSE loss between \mathbf{x} and $\hat{\mathbf{x}}$ to learn the backward process¹. For both forward and backward, the INN uses the same weights, and, therefore, the training jointly optimizes the forward and backward process.

The architecture of our INN bases on RealNVP [9] and consists of two reversible blocks with permutation layers [2]. A reversible block is composed of two complementary affine transformations, with scales s_i and translations t_i ($i \in \{1, 2\}$). The transformations describe the forward pass as

$$\mathbf{v}_1 = \mathbf{u}_1 \odot \exp(s_2(\mathbf{u}_2)) + t_2(\mathbf{u}_2), \quad \mathbf{v}_2 = \mathbf{u}_2 \odot \exp(s_1(\mathbf{v}_1)) + t_1(\mathbf{v}_1),$$

where $\mathbf{u} = [\mathbf{u}_1, \mathbf{u}_2]$ and $\mathbf{v} = [\mathbf{v}_1, \mathbf{v}_2]$ are the input and output split into halves, and \odot is the Hadamard product. The reversibility of the affine transformations ensure the invertibility of the reversible block, such that the inverse is given by

$$\mathbf{u}_2 = (\mathbf{v}_2 - t_1(\mathbf{v}_1)) \odot \exp(-s_1(\mathbf{v}_1)), \quad \mathbf{u}_1 = (\mathbf{v}_1 - t_2(\mathbf{u}_2)) \odot \exp(-s_2(\mathbf{u}_2)).$$

As a consequence, the operations s and t do not need to be invertible themselves. For each s_i and t_i , we use two fully-connected layers, with 128 neurons each, followed by ReLU and linear activation, respectively. The permutation layers enforce a different split of the halves in every reversible block [2]. We remark that we zero-pad the input \mathbf{x} to match the dimensionality of \mathbf{y} . Generally, such INN architectures have been shown to be suitable to solve diverse inverse problems [2], including problems in medical imaging [1].

2.2 MR Fingerprinting Sequence

In the context of our clinical scope, we use MRF T1-FF [17], a MRF sequence designed for the quantification of T1 relaxation time (T1) and fat fraction (FF) in fatty infiltrated tissues such as diseased skeletal muscle. Since fat can heavily

¹ The MSE loss was empirically found to be beneficial although the backward process is theoretically learned through the bijectivity property of the INN.

bias the T1 quantification, MRF T1-FF separately estimates the T1 of water ($T1_{\text{H}_2\text{O}}$) and T1 of fat ($T1_{\text{fat}}$) pools. Additionally, the confounding effects of static magnetic field inhomogeneity (Δf) and flip angle efficacy (B1) are quantified, resulting in a total of $M = 5$ MR parameters (FF, $T1_{\text{H}_2\text{O}}$, $T1_{\text{fat}}$, Δf , and B1). Fingerprints are simulated using the Bloch equations with varying MRF sequence schedules of flip angles, echo times and repetition times, resulting in fingerprints of length $T = 175$.

Two dictionaries were simulated, one for training and the other for validation and testing. The training dictionary was simulated with (start:increment:stop) (0.0:0.1:1.0) for FF, (500:100:1700, 1900:200:3100) ms for $T1_{\text{H}_2\text{O}}$, (200:25:400) ms for $T1_{\text{fat}}$, (-120:10:120) Hz for Δf , and (0.3:0.1:1.0) for B1. The other dictionary was simulated with (0.05:0.1:0.95) for FF, (550:200:1750, 2150:400:2950) ms for $T1_{\text{H}_2\text{O}}$, (215:50:365) ms for $T1_{\text{fat}}$, (-115:20:105) Hz for Δf , and (0.35:0.1:0.95) for B1, of which randomly 20 % of the entries were used for validation and the remaining 80 % for testing. In total, 396000 entries were used for training, 6720 for validation, and 26880 unseen entries for testing.

2.3 Baselines and Training

We compared the INN to five baselines, one ablation and four competing NN-based methods. The ablation, termed INN_{bwd} , uses exactly the same architecture as INN but was only trained on the backward process to ablate the benefit of jointly learning the forward and backward process. The competing methods are: (i) a fully-connected NN by Cohen et al. [8] with two hidden layers, (ii) a NN by Hoppe et al. [14] consisting of four convolution layers followed by four fully-connected layer, (iii) a recurrent NN by Oksuz et al. [19] based on gated recurrent units with 100 recurrent layers followed by a fully-connected layer, and (iv) a 1-D residual convolutional NN by Song et al. [21].

All NNs were trained using a MSE loss with an Adam optimizer [15] with the learning rate chosen from $\{0.01, 0.001, 0.0005, 0.0001\}$, and $\beta_1 = 0.9, \beta_2 = 0.999$. We trained for 80 epochs and chose the batch size from $\{50, 200\}$. At each epoch, the coefficient of determination (R^2) between \mathbf{x} and $\hat{\mathbf{x}}$ on the validation set was calculated and the best model was used for testing. As input, the real and imaginary parts of the complex-valued fingerprints \mathbf{y} were concatenated, as commonly done [5,10,4,3,14], resulting in an input dimension of $2T = 350$ in all experiments. The output dimension was $M = 5$, resulting in a zero padding of \mathbf{x} for the INN of $2T - M = 345$. As data augmentation, the fingerprints \mathbf{y} were perturbed with random noise $\mathcal{N}(0, N^2)$. The noise standard deviation N was set to imitate signal-to-noise ratio (SNR) conditions of MRF T1-FF scans. The SNR (in dB) was defined as $20 \log_{10}(S/N)$, where S is the mean intensity of the magnitude of the magnetization at thermal equilibrium in healthy skeletal muscle. N was set to 0.003 for training, and \mathbf{y} was perturbed for both the forward and backward process when training the INN. As no public code was available for the competing NNs, we implemented them in PyTorch 1.3 along with the INN. We release the code at <http://www.github.com/fabianbalsiger/mrf-reconstruction-mlmir2020>.

3 Experiments and Results

3.1 Backward Process: MR Parameter Estimation

The results of the MR parameter estimation from unperturbed fingerprints \mathbf{y} are summarized in Table 1. The mean absolute error (MAE), the mean relative error (MRE), and the R^2 between the reference \mathbf{x} and predicted $\hat{\mathbf{x}}$ MR parameters were calculated. The INN estimated all MR parameters with the highest accuracy except for the MR parameter Δf , where the INN_{bwd} yielded the best estimations in terms of MAE. Overall, all methods performed in a similar range for FF, Δf , and B1. However, a benefit in learning the Bloch simulations accentuated especially for $T1_{\text{H}_2\text{O}}$ and $T1_{\text{fat}}$, where the INN outperformed all competing methods including the ablation by a considerable margin. We analyze this behaviour in more detail in Sec. 3.2.

Robustness to noise is of considerable importance for MRF reconstruction applied to *in vivo* MRF acquisitions due to high undersampling. To simulate undersampling conditions, the performance of the INN, the INN_{bwd} , and the best competing method (Cohen et al. [8]) were analyzed under varying SNR levels, see Fig. 2. For each SNR level, we performed Monte Carlo simulations perturbing the fingerprints \mathbf{y} with 100 random noise samples. It is notable that the INN more accurately and precisely estimated the MR parameters at higher SNR levels (> 25 dB) than the other methods. At lower SNR levels, the differences between the methods became negligible, indicating that the benefit of learning the forward pass vanishes as the noise level increases. The plots for the MR parameters Δf and B1 look similar, and are omitted due to space constraints.

The inference time of the INN was approximately 50 milliseconds for 1000 fingerprints, which is in-line with the competing methods. Only the training time was approximately doubled with 5 minutes for one epoch compared to the competing methods. The number of parameters were 0.36 million for the INN

Table 1. Mean absolute error (MAE), mean relative error (MRE), and the coefficient of determination (R^2) of the MR parameter estimation from unperturbed fingerprints. a.u.: arbitrary unit.

Metric	MR parameter	Method					
		INN	INN_{bwd}	Cohen et al.	Hoppe et al.	Oksuz et al.	Song et al.
MAE	FF	0.008 \pm 0.007	0.013 \pm 0.010	0.013 \pm 0.011	0.016 \pm 0.012	0.015 \pm 0.012	0.015 \pm 0.012
	$T1_{\text{H}_2\text{O}}$ (ms)	88.9 \pm 170.2	143.2 \pm 249.3	140.6 \pm 234.8	162.2 \pm 241.8	176.0 \pm 239.8	160.1 \pm 243.5
	$T1_{\text{fat}}$ (ms)	20.8 \pm 19.4	27.8 \pm 21.6	27.9 \pm 22.0	29.0 \pm 22.1	31.7 \pm 23.0	28.1 \pm 22.8
	Δf (Hz)	0.736 \pm 0.666	0.665 \pm 0.490	0.833 \pm 0.612	2.635 \pm 1.503	1.380 \pm 1.083	1.532 \pm 1.169
	B1 (a.u.)	0.012 \pm 0.010	0.013 \pm 0.010	0.015 \pm 0.013	0.016 \pm 0.014	0.027 \pm 0.021	0.019 \pm 0.014
MRE	FF (%)	2.89 \pm 4.69	4.23 \pm 5.62	4.09 \pm 5.02	5.64 \pm 7.62	5.10 \pm 6.99	6.33 \pm 11.94
	$T1_{\text{H}_2\text{O}}$ (%)	6.75 \pm 15.46	11.55 \pm 27.23	11.47 \pm 25.21	12.66 \pm 25.22	13.32 \pm 23.07	13.36 \pm 27.42
	$T1_{\text{fat}}$ (%)	7.48 \pm 7.28	10.34 \pm 9.22	10.33 \pm 9.40	10.97 \pm 9.80	11.96 \pm 10.27	10.41 \pm 9.81
	Δf (%)	2.50 \pm 5.00	2.86 \pm 6.07	3.16 \pm 5.91	7.52 \pm 11.40	3.71 \pm 5.40	5.19 \pm 9.00
	B1 (%)	1.98 \pm 1.95	2.17 \pm 1.88	2.56 \pm 2.34	2.83 \pm 2.91	4.22 \pm 3.01	3.18 \pm 2.69
R^2	FF	0.999	0.997	0.996	0.995	0.995	0.995
	$T1_{\text{H}_2\text{O}}$	0.934	0.852	0.866	0.848	0.841	0.848
	$T1_{\text{fat}}$	0.741	0.604	0.596	0.574	0.508	0.582
	Δf	1.000	1.000	1.000	0.998	0.999	0.999
	B1	0.994	0.993	0.990	0.988	0.972	0.986

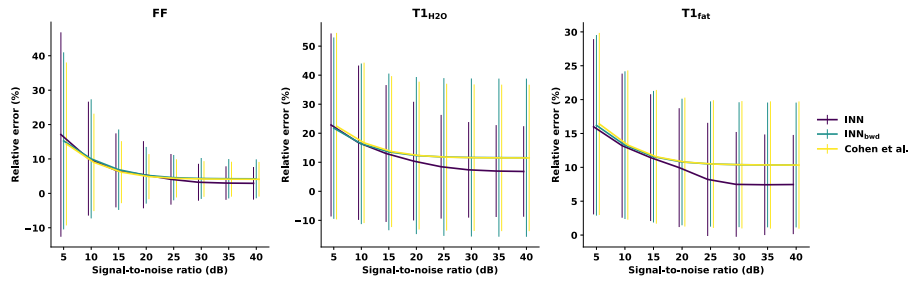


Fig. 2. Reconstruction performance in mean relative error of the INN, INN_{bwd} , and Cohen et al. [8] under varying SNR conditions for the MR parameters FF, $T1_{\text{H}_2\text{O}}$, and $T1_{\text{fat}}$. Error bars indicate \pm standard deviation. An SNR level of approximately 20 dB can be considered similar to an *in vivo* MRF T1-FF scan.

and INN_{bwd} , 0.20 million for Cohen et al. [8], 6.56 million for Hoppe et al. [14], 0.12 million for Oksuz et al. [19], and 1.49 million for Song et al. [21].

3.2 Forward Process: Benefit of Learning Bloch Simulations

Jointly learning the forward process mainly benefits estimating $T1_{\text{H}_2\text{O}}$ and $T1_{\text{fat}}$ (cf. Table 1). To analyze this benefit, we need to introduce MR physics in presence of fat. The used sequence MRF T1-FF is designed for T1 quantification in fatty infiltrated tissues where the fat infiltration occurs at varying fractions, from no fat ($\text{FF}=0.0$), to being solely fat ($\text{FF}=1.0$). Unfortunately, fat infiltration, and therefore FF, greatly affects T1 quantification [18]. At $\text{FF}=1.0$, $T1_{\text{H}_2\text{O}}$ is not measurable as no water is present. Similarly, at $\text{FF}=0.0$, $T1_{\text{fat}}$ is not measurable as no fat is present. Generally, estimating $T1_{\text{H}_2\text{O}}$ is difficult at high FF values as the pooled (or global) T1 is heavily biased by the $T1_{\text{fat}}$. Contrarily, at low FF values, estimating $T1_{\text{fat}}$ is difficult as almost no fat is present. Learning the forward process could especially benefit such cases, i.e., when the information in the fingerprints is ambiguous due to MR physical restrictions. To test this assumption, we calculated the difference between the relative errors of the INN_{bwd} and INN. The heat maps in Fig. 3 show the differences for estimated $T1_{\text{H}_2\text{O}}$ and $T1_{\text{fat}}$ at varying FF and $T1_{\text{H}_2\text{O}}$ values. On the one hand, the forward process helped at estimating short $T1_{\text{H}_2\text{O}}$ (< 1000 ms) at high FF more accurately than INN_{bwd} , Fig. 3 left. Short $T1_{\text{H}_2\text{O}}$ values are especially difficult to differentiate from $T1_{\text{fat}}$, as these are also very short (cf. dictionary ranges in Sec. 2.2). On the other hand, the forward process benefited the estimation of $T1_{\text{fat}}$ values at lower FF (< 0.5), Fig. 3 right. At the very low FF of 0.05, the benefit diminished as it seems difficult to discriminate short $T1_{\text{fat}}$ values from longer $T1_{\text{H}_2\text{O}}$ values, even when the forward process was learned. A nearly identical pattern was also obtained when comparing the INN with the method of Cohen et al. [8] (not shown). These results indicate that learning the forward process helps disentangling underlying MR physical processes.

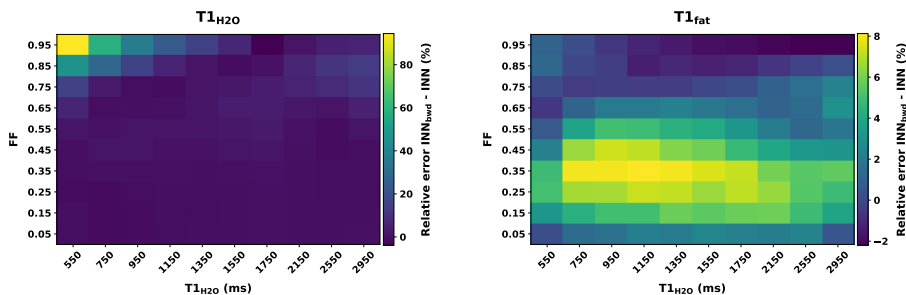


Fig. 3. Heat maps of the relative error differences between INN_{bwd} and INN for the MR parameters $T1_{H_2O}$ (left) and $T1_{fat}$ (right). Positive values indicate better performance of the INN .

3.3 Relation between the Forward and Backward Process

Learning the Bloch simulations benefits not only the MR parameter estimations but could also foster interpretability of the estimation. Due to the cyclic nature of the INN , large errors in the backward process, i.e., the error between \mathbf{x} and $\hat{\mathbf{x}}$, should be associated with large errors in the forward process, i.e., the error between \mathbf{y} and $\hat{\mathbf{y}}$. We tested this hypothesis by analyzing the correlation of the MRE between \mathbf{x} and $\hat{\mathbf{x}}$ and the inner product between the fingerprints \mathbf{y} and $\hat{\mathbf{y}}$. The association between the MRE and the inner product is shown in the scatter plot of Fig. 4. The Spearman rank-order correlation coefficient was -0.301 ($p < 0.001$), indicating a weak monotonic relationship. A high and a low error example are shown on the right-hand side of Fig. 4. The lower agreement between \mathbf{y} and $\hat{\mathbf{y}}$ of the high error example is visually noticeable compared to the low error example. The main source of error is the $T1_{H_2O}$, which is difficult to estimate at the high FF of 0.95 the fingerprint \mathbf{y} was simulated with.

4 Discussion and Conclusion

We revisited NN-based MRF reconstruction by formulating it as an inverse problem. The INN allows to jointly learn the forward process from MR parameters to fingerprints and the backward process from fingerprints to MR parameters. Regarding reconstruction performance, our results suggest that learning the Bloch simulations is beneficial for MR parameter estimation.

Our experiments showed that the benefit of the INN is considerable when the information in the fingerprints is ambiguous due to MR physical restrictions. Independent of the method (invertible, fully-connected, convolutional, or recurrent) and the network size (number of parameters), FF, Δf , and B1 were nearly identically well estimated. The errors for these MR parameters were below a step size to simulate dictionaries of reasonable size for the computational intensive dictionary matching. However, this is not the case for $T1_{H_2O}$ and $T1_{fat}$, where the INN performs superior. By ablation, we could attribute this performance

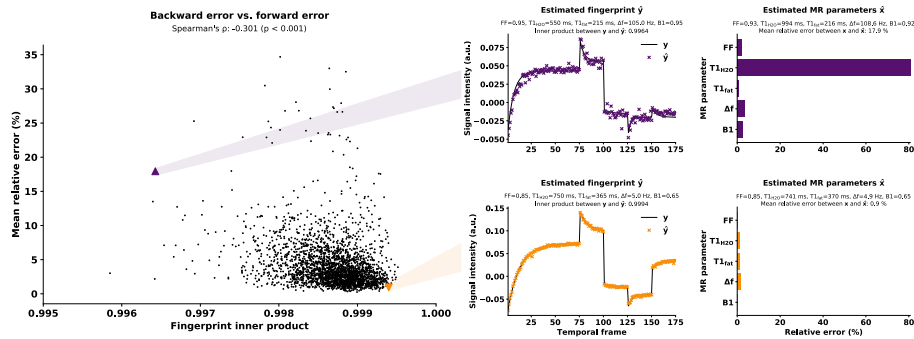


Fig. 4. Scatter plot relating the error in the forward and the backward process. For a pair (\mathbf{x}, \mathbf{y}) , we calculated $(\hat{\mathbf{x}}, \hat{\mathbf{y}})$ using the INN and plotted the mean relative error between \mathbf{x} and $\hat{\mathbf{x}}$ versus the inner product between \mathbf{y} and $\hat{\mathbf{y}}$. The fingerprints and the relative errors of a high (\blacktriangle) and a low (\blacktriangledown) error example are shown on the right-hand side. For visualization purposes, only a random subset of 10 % of the data points in the scatter plot and the real part of the fingerprints were plotted. a.u.: arbitrary unit.

gain to the learning of the forward process. This insight might have implications beyond T1 and FF quantification, e.g., for fast imaging with steady-state precession (FISP) sequences, where T2 relaxation time quantification is more difficult than T1 quantification [8,10,14,11]. Further, the interplay between the forward and backward process enable an enhanced interpretability of the method, which might be regarded as reconstruction uncertainty. This might be useful for MRF sequence design and optimization targeted to NN-based reconstruction.

The main limitation of this proof-of-concept study is clearly that the method was not applied to *in vivo* MRF acquisitions. Prior to doing, the behaviour of the INN under heavy noise conditions needs to be further investigated. It is currently unclear, as to why the benefit of the forward process diminishes at lower SNR levels (cf. Fig. 2). The simplest explanation is clearly the lack of enough signal, which makes MR parameter estimation difficult, independent of the method. Here, spatial regularization would most likely help [4,3], which is also possible with INNs. First attempts in this direction are promising.

In conclusion, we showed that jointly learning the forward and backward process benefits the reconstruction of MRF. INNs are suitable for such joint learning and might be a feasible alternative to the current solely backward-based NNs for MRF reconstruction.

Acknowledgement. This research was supported by the Swiss National Science Foundation (SNSF). The authors thank the NVIDIA Corporation for their GPU donation.

References

1. Adler, T.J., Ardizzone, L., Vemuri, A., Ayala, L., Gröhl, J., Kirchner, T., Wirkert, S., Kruse, J., Rother, C., Köthe, U., Maier-Hein, L.: Uncertainty-aware performance assessment of optical imaging modalities with invertible neural networks. *International Journal of Computer Assisted Radiology and Surgery* **14**(6), 997–1007 (2019). <https://doi.org/10.1007/s11548-019-01939-9>
2. Ardizzone, L., Kruse, J., Wirkert, S., Rahner, D., Pellegrini, E.W., Klessen, R.S., Maier-Hein, L., Rother, C., Köthe, U.: Analyzing Inverse Problems with Invertible Neural Networks. In: *International Conference on Learning Representations* (2019)
3. Balsiger, F., Jungo, A., Scheidegger, O., Carlier, P.G., Reyes, M., Marty, B.: Spatially Regularized Parametric Map Reconstruction for Fast Magnetic Resonance Fingerprinting. *Medical Image Analysis* **64**, 101741 (2020). <https://doi.org/10.1016/j.media.2020.101741>
4. Balsiger, F., Scheidegger, O., Carlier, P.G., Marty, B., Reyes, M.: On the Spatial and Temporal Influence for the Reconstruction of Magnetic Resonance Fingerprinting. In: Cardoso, M.J., Feragen, A., Glocker, B., Konukoglu, E., Oguz, I., Unal, G., Vercauteren, T. (eds.) *Proceedings of The 2nd International Conference on Medical Imaging with Deep Learning*. *Proceedings of Machine Learning Research*, vol. 102, pp. 27–38. PMLR, London (2019)
5. Balsiger, F., Shridhar Konar, A., Chikop, S., Chandran, V., Scheidegger, O., Geethanath, S., Reyes, M.: Magnetic Resonance Fingerprinting Reconstruction via Spatiotemporal Convolutional Neural Networks. In: Knoll, F., Maier, A., Rueckert, D. (eds.) *Machine Learning for Medical Image Reconstruction*, *Lecture Notes in Computer Science*, vol. 11074, pp. 39–46. Springer, Cham (2018). https://doi.org/10.1007/978-3-030-00129-2_5
6. Bloch, F.: Nuclear induction. *Physical Review* **70**(7-8), 460–474 (1946). <https://doi.org/10.1103/PhysRev.70.460>
7. Boux, F., Forbes, F., Arbel, J., Lemasson, B., Barbier, E.: Bayesian inverse regression for vascular magnetic resonance fingerprinting. HAL preprint hal-02314026v2 (2020)
8. Cohen, O., Zhu, B., Rosen, M.S.: MR fingerprinting Deep RecOnstruction Network (DRONE). *Magnetic Resonance in Medicine* **80**(3), 885–894 (2018). <https://doi.org/10.1002/mrm.27198>
9. Dinh, L., Sohl-Dickstein, J., Bengio, S.: Density Estimation Using Real NVP. In: *International Conference on Learning Representations* (2017)
10. Fang, Z., Chen, Y., Liu, M., Xiang, L., Zhang, Q., Wang, Q., Lin, W., Shen, D.: Deep Learning for Fast and Spatially-Constrained Tissue Quantification from Highly-Accelerated Data in Magnetic Resonance Fingerprinting. *IEEE Transactions on Medical Imaging* **38**(10), 2364–2374 (2019). <https://doi.org/10.1109/TMI.2019.2899328>
11. Fang, Z., Chen, Y., Nie, D., Lin, W., Shen, D.: RCA-U-Net: Residual Channel Attention U-Net for Fast Tissue Quantification in Magnetic Resonance Fingerprinting. In: Shen, D., Liu, T., Peters, T.M., Staib, L.H., Essert, C., Zhou, S., Yap, P.T., Khan, A. (eds.) *Medical Image Computing and Computer Assisted Intervention – MICCAI 2019*. *Lecture Notes in Computer Science*, vol. 11766, pp. 101–109. Springer (2019). https://doi.org/10.1007/978-3-030-32248-9_12
12. Golbabaee, M., Chen, D., Gómez, P.A., Menzel, M.I., Davies, M.E.: Geometry of Deep Learning for Magnetic Resonance Fingerprinting. In: *IEEE International Conference on Acoustics, Speech and Signal Processing (ICASSP)*. pp. 7825–7829. IEEE (2019). <https://doi.org/10.1109/ICASSP.2019.8683549>

13. Hoppe, E., Körzdörfer, G., Würfl, T., Wetzl, J., Lugauer, F., Pfeuffer, J., Maier, A.: Deep Learning for Magnetic Resonance Fingerprinting: A New Approach for Predicting Quantitative Parameter Values from Time Series. In: Röhrig, R., Timmer, A., Binder, H., Sax, U. (eds.) *German Medical Data Sciences: Visions and Bridges*. vol. 243, pp. 202–206. Oldenburg, Oldenburg (2017). <https://doi.org/10.3233/978-1-61499-808-2-202>
14. Hoppe, E., Thamm, F., Körzdörfer, G., Syben, C., Schirmacher, F., Nittka, M., Pfeuffer, J., Meyer, H., Maier, A.: RinQ Fingerprinting: Recurrence-Informed Quantile Networks for Magnetic Resonance Fingerprinting. In: Shen, D., Liu, T., Peters, T.M., Staib, L.H., Essert, C., Zhou, S., Yap, P.T., Khan, A. (eds.) *Medical Image Computing and Computer Assisted Intervention – MICCAI 2019*. *Lecture Notes in Computer Science*, vol. 11766, pp. 92–100. Springer (2019). https://doi.org/10.1007/978-3-030-32248-9_11
15. Kingma, D.P., Ba, J.L.: Adam: A Method for Stochastic Optimization. In: *International Conference on Learning Representations* (2015)
16. Ma, D., Gulani, V., Seiberlich, N., Liu, K., Sunshine, J.L., Duerk, J.L., Griswold, M.A.: Magnetic resonance fingerprinting. *Nature* **495**(7440), 187–192 (2013). <https://doi.org/10.1038/nature11971>
17. Marty, B., Carlier, P.G.: MR fingerprinting for water T1 and fat fraction quantification in fat infiltrated skeletal muscles. *Magnetic Resonance in Medicine* **83**(2), 621–634 (2019). <https://doi.org/10.1002/mrm.27960>
18. Marty, B., Coppa, B., Carlier, P.G.: Monitoring skeletal muscle chronic fatty degenerations with fast T1-mapping. *European Radiology* **28**(11), 4662–4668 (2018). <https://doi.org/10.1007/s00330-018-5433-z>
19. Oksuz, I., Cruz, G., Clough, J., Bustin, A., Fuin, N., Botnar, R.M., Prieto, C., King, A.P., Schnabel, J.A.: Magnetic Resonance Fingerprinting using Recurrent Neural Networks. In: *International Symposium on Biomedical Imaging*. pp. 1537–1540. IEEE (2019). <https://doi.org/10.1109/ISBI.2019.8759502>
20. Poorman, M.E., Martin, M.N., Ma, D., McGivney, D.F., Gulani, V., Griswold, M.A., Keenan, K.E.: Magnetic resonance fingerprinting Part 1: Potential uses, current challenges, and recommendations. *Journal of Magnetic Resonance Imaging* **51**(3), 675–692 (2019). <https://doi.org/10.1002/jmri.26836>
21. Song, P., Eldar, Y.C., Mazor, G., Rodrigues, M.R.: HYDRA: Hybrid Deep Magnetic Resonance Fingerprinting. *Medical Physics* **46**(11), 4951–4969 (2019). <https://doi.org/10.1002/mp.13727>